

# Validation of model-simulated sea surface current and sea surface temperature with observations in the Southern Indian Ocean

Anshu Prakash Mishra<sup>1,3,\*</sup>, S. Rai<sup>1</sup> and A. C. Pandey<sup>1,2</sup>

<sup>1</sup>K. Banerjee Centre of Atmospheric and Ocean Studies, Nehru Science Centre, Faculty of Science, University of Allahabad and

<sup>2</sup>Department of Physics, University of Allahabad, Allahabad 211 002, India

<sup>3</sup>Present address: Central Water Commission, Upper Brahmaputra Division, J. P. Nagar, PO CR Building, Dibrugarh 786 003, India

**A 25-layer Ocean General Circulation Model has been used to investigate and analyse the model-simulated sea surface current (SSC) and sea surface temperature (SST) fields from a 26-year model simulation covering the Southern Indian Ocean region (50°S–10°N and 30–120°E). In general, simulated time-mean SSC and SST fields are found to agree well with the corresponding observed datasets in most parts of the model domain. All major currents such as Antarctic Circumpolar Current, Equatorial Counter Current, South Equatorial Current, North Equatorial Current and Agulhas Current are preserved in the model, as verified by the observation. However, slight variation in current intensity is reflected on monthly scale. Similarly, the pattern of time-mean monthly SST field is found to agree with Levitus climatology. However, disparities do exist as evidenced by the SST bias calculation in some parts of the model domain. The vertical profile of temperature from the model simulation is found to agree well with the Levitus climatology. We conclude that the model is able to reproduce well, the observed structure in the ocean.**

**Keywords:** Antarctic Circumpolar Current, sea surface current, sea surface temperature, South Equatorial Current, Southern Indian Ocean.

THE influence of numerical modelling has grown dramatically over the last few decades due to the advent of faster computational resources and improved methods. The practice of oceanic numerical modelling is growing rapidly because of a widespread realization that model solutions can, either now or at least in the near future, be skillful in mimicking observed oceanic features with the exploitation of steady increase in computing power that makes meaningful simulation of oceanic circulation more feasible. Ocean General Circulation Models (OGCMs) are useful because they enable the study of the ocean currents in the context of a dynamically consistent model-simulated dataset. They

also have many other important applications, viz. dynamical coupling with the atmosphere, sea-ice, land run-off, etc.<sup>1</sup>.

Knowledge of ocean variables, viz. sea surface current (SSC) and sea surface temperature (SST), aids in understanding features like mesoscale gyres and further improves our understanding of climate-related studies. Oceanic currents are described as coherent horizontal movement of water that flow in complex patterns affected by wind, water salinity, heat content, bottom topography and earth's rotation. Due to extent of the earth's oceans, measurement of ocean current by ship drift or ocean drifter buoys is difficult, especially south of 50°S; the fields are not reliable. However, ocean-current measurements can be achieved from a variety of current meters<sup>2</sup>. The vector measuring current meter<sup>3</sup> and the acoustic Doppler current profiler<sup>4,5</sup> have been extensively used by oceanographers during the past decade. In particular, these instruments have proven to be reliable for obtaining quality ocean-current data from moorings for scientific studies<sup>2,6–8</sup>.

A validation study using the 25 layer OGCM model was performed. Parameters like SSC and SST were chosen to skill assess the model performance with observations. The study also analysed how these oceanic variables in the model simulations compare with the observations; for example, what scientific questions about validation can the model answer?

A 26-year numerical simulation of Modular Ocean Model (MOM3.0) was performed by forcing the model with a climatological monthly wind stress from the NCEP–NCAR reanalysis. This study presents an evaluation of the Southern Indian Ocean (SIO; 30°E–120°E, 50°S–10°N) time-mean velocity field (1900–25; on a monthly and an annual mean timescale) and time-mean SST field (on a monthly timescale) from the 26-year integration by comparing these fields with ship drift observation (1° × 1°) datasets<sup>9–11</sup> for the velocity field and Levitus climatology<sup>12</sup> (1° × 1°) for the SST field. In the ship drift observed data, each velocity component was estimated using the scalar objective analysis (OA) routine described in Mariano and Brown<sup>11</sup>, after a median filter<sup>13</sup> was applied to the data to remove gross outliers.

\*For correspondence. (e-mail: anshu\_786@rediffmail.com)

## Model description

The OGCM used in this study is version 3 of the GFDL MOM<sup>14–16</sup>. This version uses the Boussinesq and traditional approximations, and allows use of rigid-lid and free-surface methods. The horizontal mixing of tracers and momentum is Laplacian. Momentum mixing uses the space-time-dependent scheme of Smagorinsky<sup>17</sup> and tracer mixing uses Redi<sup>18</sup> diffusion along with quasi-adiabatic stirring of Gent and McWilliams<sup>19</sup>. Its domain is that of the world oceans between 74.25°S and 65°N. The zonal resolution is 1.5°. The meridional resolution is 0.5° between 10°N and 10°S, gradually increasing to 1.5° at 20°N and 20°S. There are 25 levels in the vertical with 17 levels in the upper 450 m of the ocean. The model is forced by the monthly averaged surface wind stress from the NCEP–NCAR reanalysis. The original surface reanalysis is on an irregular grid with a zonal resolution of 1.875° and Gaussian latitudes of grid spacing less than 2°, and is linearly interpolated to the OGCM grids. The vertical mixing scheme is non-local K-profile parameterization (KPP) of Large *et al.*<sup>20</sup>. The model surface salinity is relaxed to Levitus monthly climatology<sup>21</sup>.

For a quantitative evaluation of the model performance, some statistical measures and skill assessment have been done in the present study. Several skill measurement and statistical studies<sup>22,23</sup> have been performed by various re-

searchers in the diverse regions of global and regional oceans using MOM3.0, and results have been validated against other models. Since the accuracy of the atmospheric forcing and climatologies of the SST can strongly affect quantitative measures of the model simulation skill, high model simulation skill is also an assessment of these factors to a limited extent. It would be difficult to obtain high model accuracy over diverse regimes of the global ocean with highly inaccurate data<sup>24</sup>. NCEP and NCAR<sup>25</sup> are cooperating in a project (denoted ‘reanalysis’) to produce a 40-year record of global analyses of atmospheric fields in support of needs of research and climate monitoring communities. This effort involves the recovery of land surface, ship, rawinsonde, aircraft, satellite and other data; quality control and assimilation of these data with a data assimilation system that is kept unchanged over the reanalysis period 1957–96. The NCEP/NCAR reanalysis, which is currently available back to 1948, contains several meteorological parameters in a global spatial resolution of 2.5° × 2.5° (lat. × long.) and in a vertical extent from the surface toward the 10 hPa level. Therefore, the NCEP/NCAR reanalysis offers potentially an opportunity to investigate the long-term variability of the troposphere and stratospheric climate as well as the connection between both in a global scale. For this purpose, these data are extensively used worldwide.

## Results and discussion

The ability of model to reproduce climatological SSC is first evaluated in terms of the annual mean using the climatological ship-drift dataset (Figure 1 *b*) and the corresponding model simulated sea surface circulation (Figure 1 *a*). The horizontal mean sea surface circulation (Figure 1 *a*) is comparable with the observation (Figure 1 *b*), with the evidence of major currents such as Antarctic Circumpolar Current (ACC) in the circumpolar region (around 40°S and poleward), the Equatorial Current, and the Equatorial Counter Current (ECC). However, the magnitude of surface current in the model (Figure 1 *a*) is weaker compared to the observation (Figure 1 *b*). This may be because of the differences in the resolution of the model and the ship-drift data. Moreover, the ship-drift data may not be accurate because of certain limitations and technique applied for interpolation, whereas the model simulation may also show deficiency in forcing fields and boundary condition. This may lead to differences in the magnitude of the currents. The general circulation of currents at the sea surface is of a zonal nature, particularly the ACC. The nature of the model circulation seems similar to the observation, which is attributed to the fact that the stable ACC serves as a major circulation element<sup>26</sup>. The South Equatorial Current (SEC) near 10°S–20°S, 50°E–110°E is also evident in Figure 1 *a* and *b*. Almost no qualitative difference between the model (Figure 1 *a*) and observed annual mean

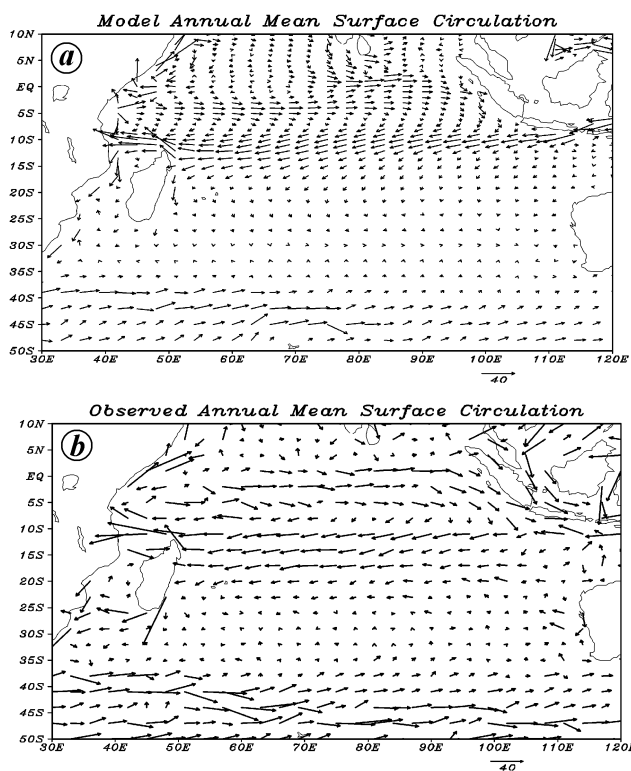


**Figure 1.** *a*, Model-simulated annual mean surface circulation ( $\text{cm s}^{-1}$ ). *b*, Ship drift observed annual mean surface circulation ( $\text{cm s}^{-1}$ ). (Arrow length of 0.5 cm represents current speed of  $40 \text{ cm s}^{-1}$ .)

sea surface circulation pattern (Figure 1*b*) is seen, excluding a narrow current at some places along the equator.

The OA routine applied in ship-drift data is used extensively by meteorologists<sup>27,28</sup> and oceanographers<sup>29,30</sup> to estimate the values of geophysical variables at a grid of interpolation points from irregularly distributed datapoints. OA is based on the Gauss–Markoff theorem<sup>11</sup> for a linear minimum mean square estimate of a random variable, and requires estimates of the first- and second-order statistics of both the observing and the dynamical system. The OA package also produces the mapping estimation error covariance and mean values for a particular field, which are used during data assimilation. The surface current measurements from ship-drift data required correction with respect to leeway in order to have a useful dataset of surface current measurements<sup>31</sup>. Also, the track of ship drift is one of the factors for performing interpolation and obtaining the correct data. Therefore, the data collected by ship drift have their limitations. Estimates remain poor in the southern Ocean due to scarcity of observation stations, and hence qualitative assessment has been done here using ship-drift data against the model results.

The sea surface circulation for January, April, July and October of the multiyear model mean is shown in Figures 2*a*, 3*a*, 4*a* and 5*a* and the corresponding observations are shown in Figures 2*b*, 3*b*, 4*b*, and 5*b* respectively. The general surface circulation scheme in January, April, July

and October is close to that obtained from the respective observations; however, the interpolated observed currents on a grid resolution of  $1^\circ \times 1^\circ$  are considerably smoothed and, thus contain only major, large gyres and currents. Comparison of current velocity intensity indicates that most currents in the model during each month have velocities/intensities within the limits obtained in the observations. The root mean square error (RMSE) has been evaluated between model output and ship-drift data at representative points in deep and shallow-water regions for January, April, July and October (Table 1). Table 1 shows that the model performs well in the deep-water region and also to some extent in shallow-water regions.

The ACC preserves its general eastward direction in the model (Figures 2*a*, 3*a*, 4*a* and 5*a*) as well as in the observations (Figures 2*b*, 3*b*, 4*b* and 5*b*) during all the months and ACC current velocities look stable and its width ranges between  $40^\circ\text{S}$  and  $60^\circ\text{S}$ . The general nature of the circulation is qualitatively alike in the model as well as in the observations during each month. The nature of the modelled ocean circulation is complicated in some places and is not consistent with the observation in a narrow belt (Figure 2*a*), which reflects peculiarities of temperature and salinity field. However, the general model circulation pattern follows the observations.

The SEC ( $10^\circ\text{S}$ – $20^\circ\text{S}$ ,  $50^\circ\text{E}$ – $110^\circ\text{E}$ ) and North Equatorial Current (NEC,  $0$ – $8^\circ\text{N}$ ,  $50^\circ\text{E}$ – $110^\circ\text{E}$ ), flowing west-

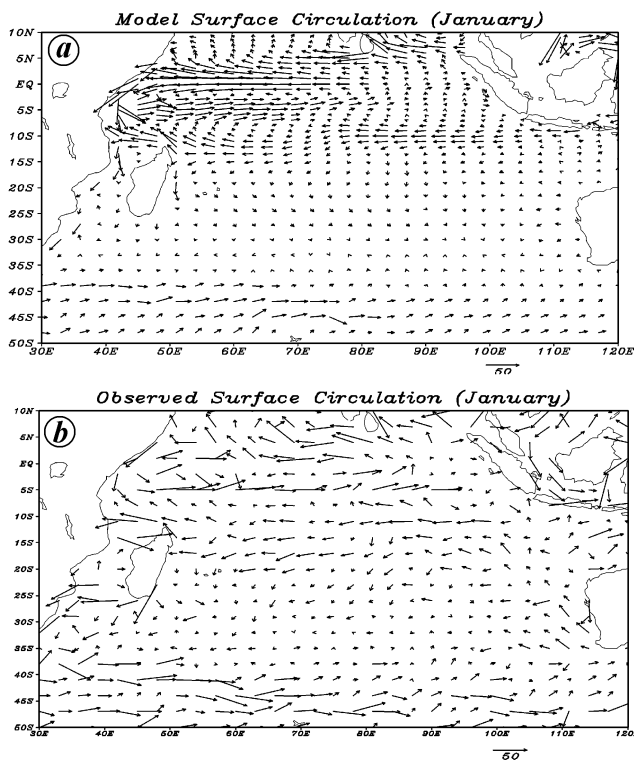


**Figure 2.** *a*, Time-mean (1900–25) SSC ( $\text{cm s}^{-1}$ ) simulated by the ocean model for January. *b*, Ship-drift observed circulation ( $\text{cm s}^{-1}$ ) for January. (Arrow length of 0.5 cm represents current speed of  $50 \text{ cm s}^{-1}$ .)

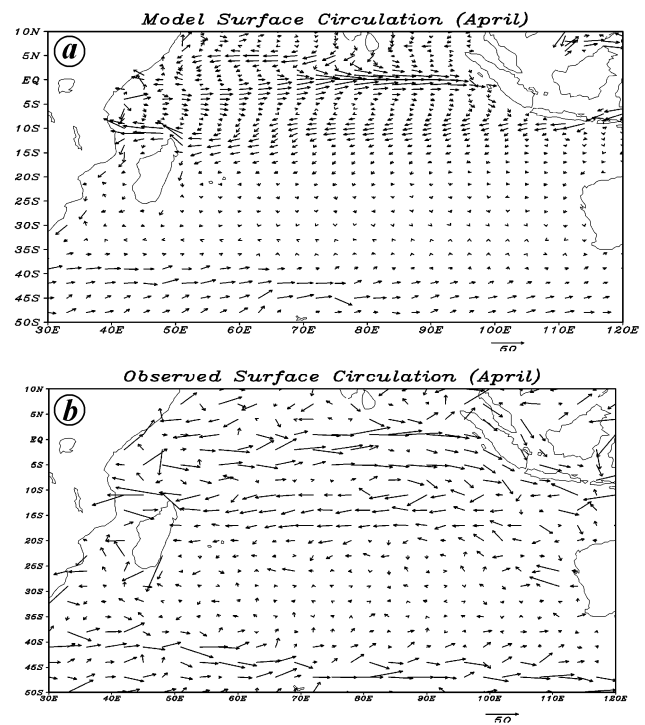


**Figure 3.** *a*, Time-mean (1900–25) SSC ( $\text{cm s}^{-1}$ ) simulated by the ocean model for April. *b*, Ship-drift observed circulation ( $\text{cm s}^{-1}$ ) for April. (Arrow length of 0.5 cm represents current speed of  $50 \text{ cm s}^{-1}$ .)

**Table 1.** RMSE evaluated at selected regions

Selected region	RMSE ( $\text{ms}^{-1}$ )		SD (standard deviation) of observed data ( $\text{ms}^{-1}$ )	
	U	V	U	V
Deep-water region ( $22^{\circ}\text{S}$ – $16^{\circ}\text{S}$ , $98^{\circ}\text{E}$ – $102^{\circ}\text{E}$ )	0.02	0.06	0.08	0.07
Shallow-water region ( $24^{\circ}\text{S}$ – $27^{\circ}\text{S}$ , $111^{\circ}\text{E}$ – $114^{\circ}\text{E}$ )	0.08	0.12	0.09	0.13
( $20^{\circ}\text{S}$ – $18^{\circ}\text{S}$ , $117^{\circ}\text{E}$ – $120^{\circ}\text{E}$ )	0.05	0.06	0.06	0.05

U, Zonal current component; V, Meridional current component.

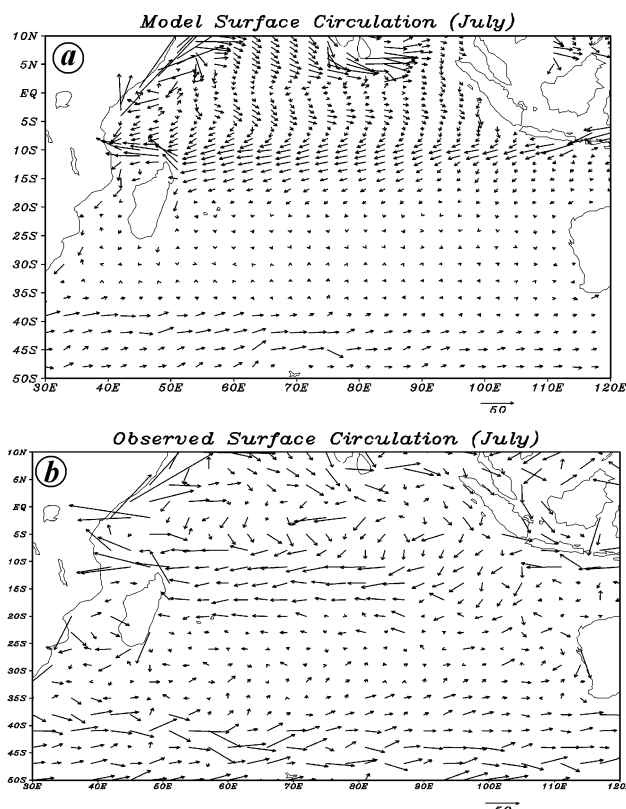


**Figure 4.** *a*, Time-mean (1900–25) SSC ( $\text{cm s}^{-1}$ ) simulated by the ocean model for July. *b*, Ship-drift observed circulation ( $\text{cm s}^{-1}$ ) for July. (Arrow length of 0.5 cm represents current speed of  $50 \text{ cm s}^{-1}$ .)

ward near the equator with a weaker eastward ECC occupying a narrow belt within  $60^{\circ}\text{E}$ – $95^{\circ}\text{E}$ ,  $0$ – $2^{\circ}\text{S}$  and flowing between them, are simulated well by the model for each month (Figures 2 *a*, 3 *a*, 4 *a* and 5 *a*; observations shown in Figures 2 *b*, 3 *b*, 4 *b* and 5 *b*). The Mozambique Current ( $10^{\circ}\text{S}$ – $30^{\circ}\text{S}$ ,  $30^{\circ}\text{E}$ – $50^{\circ}\text{E}$ ), flowing between the African coast and Madagascar through Mozambique Channel, and the Agulhas Return Current ( $30^{\circ}\text{S}$ – $40^{\circ}\text{S}$ ,  $30^{\circ}\text{E}$ – $50^{\circ}\text{E}$ ) at the southern end of Madagascar show anomaly between model computation (Figures 2 *a*, 3 *a*, 4 *a*, and 5 *a*) and ship-drift data (Figures 2 *b*, 3 *b*, 4 *b* and 5 *b*). Further, it is obvious that the model simulates the flow of the Mozambique Current well, while ship-drift data show out-of-phase flow. This mismatch is only related to observed ship-drift data, which do not simulate correctly the Mozambique Current.

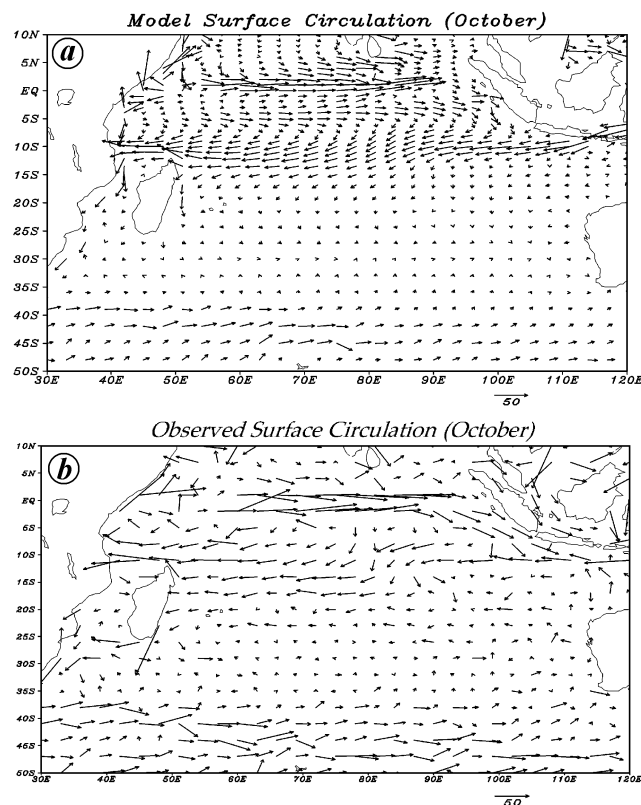


**Figure 5.** *a*, Time-mean (1900–25) SSC ( $\text{cm s}^{-1}$ ) simulated by the ocean model for October. *b*, Ship-drift observed circulation ( $\text{cm s}^{-1}$ ) for October. (Arrow length of 0.5 cm represents current speed of  $50 \text{ cm s}^{-1}$ .)

As far as the circulation in the Indian Ocean is concerned, the divergence extends from western to eastern oceanic coasts in the region defined by  $60^{\circ}\text{E}$ – $90^{\circ}\text{E}$  and  $1^{\circ}\text{S}$ – $3^{\circ}\text{S}$  (Figures 2 *a* to 5 *a*) and the southern subtropical anti-cyclonic gyre (ACG) occupies a large longitudinal width between  $5^{\circ}\text{S}$  and  $40^{\circ}\text{S}$  (Figures 2 *a*–5 *a*). These model features can also be seen in the observations (Figures 2 *b*–5 *b*). The largest gyre in the SIO is the subtropical ACG. In all three oceans, the subtropical ACG is characteristic of a common physical nature related to the available planetary anticyclonic gyre in the atmosphere and intensive processes of heating and evaporation<sup>26</sup>. In general, the correspondence of the circulation on a monthly scale seems to be good as long as observations are followed.

Figures 6 and 7 show the time-mean SST simulated by the model, corresponding observations<sup>12</sup> and SST bias for January and July respectively. The evolution of the model time-mean SST is similar to that of the observed SST for January and July with a variation around Arabian Sea, Java Sea and near coastal areas. However, the SST bias in January is within  $\pm 1^\circ\text{C}$  in most of the basins (Figure 6 c). Interestingly, major differences occur at some places in the Arabian Sea, near Java Sea and in the coastal region near Madagascar, where the model SST is higher than the Levitus climatology by  $1^\circ\text{C}$ . In the southern Ocean, maximum difference exceeding  $-1^\circ\text{C}$  is observed in the region around  $35^\circ\text{S}$ ,  $80^\circ\text{E}$ – $120^\circ\text{E}$  and near the circumpolar region ( $40^\circ\text{S}$ ,  $50^\circ\text{E}$ – $70^\circ\text{E}$ ). In July (Figure 7 c), the difference is within  $\pm 1^\circ\text{C}$  in most of the regions, as in January. In the regions around  $55^\circ\text{E}$ – $72^\circ\text{E}$ ,  $45^\circ\text{S}$ – $50^\circ\text{S}$  and  $20^\circ\text{S}$ – $35^\circ\text{S}$ ,  $90^\circ\text{E}$ – $110^\circ\text{E}$ , SST bias is  $-1^\circ\text{C}$  (i.e. the model SST is lower than the Levitus climatology by about  $1^\circ\text{C}$ ) and regions around Arabian Sea, Java Sea and the coastal region near Madagascar show differences up to  $1^\circ\text{C}$ , i.e. the model SST is higher than the Levitus climatology by about  $1^\circ\text{C}$ . In general, we find that the ocean model has a warm bias along the coasts and cool bias away from the coasts (near the middle of the ocean), and SST bias is  $\pm 1^\circ\text{C}$  in most of the basins

in January as well as in July. These biases may be due to some deficiency in the forcing field as well as in model configuration and coarser resolution of the model domain. In the model, the following elucidate the role of the forcing mechanism: (i) the surface forcing of wind stress from NCEP/NCAR and (ii) heat flux parameterized through damping of SST. The NCEP/NCAR forcing may be considered less accurate forcing field<sup>32</sup> and thermal forcing is also treated as 'poor'. Due to this reason, ocean modellers often relax the ocean model simulation to the observed SST. However, various forcing fields applied in the model put a limitation for a certain model results and this differs from data to data. The model provides the result using natural scientific equations under specific forcing applied in the model. In the present work, the biases are within  $+1$  to  $-1$  in most of the basins as far as model simulations and their comparisons are concerned. There is scope for improvement of the model results provided one performs long-term simulations by changing the mechanism of forcing fields. Then one can assess the capability of model accuracy in the simulation against the observation in the context of the biases observed in the simulation. It is difficult to discuss further the deficiency in the forcing field and model performance due to limitations of the various datasets.

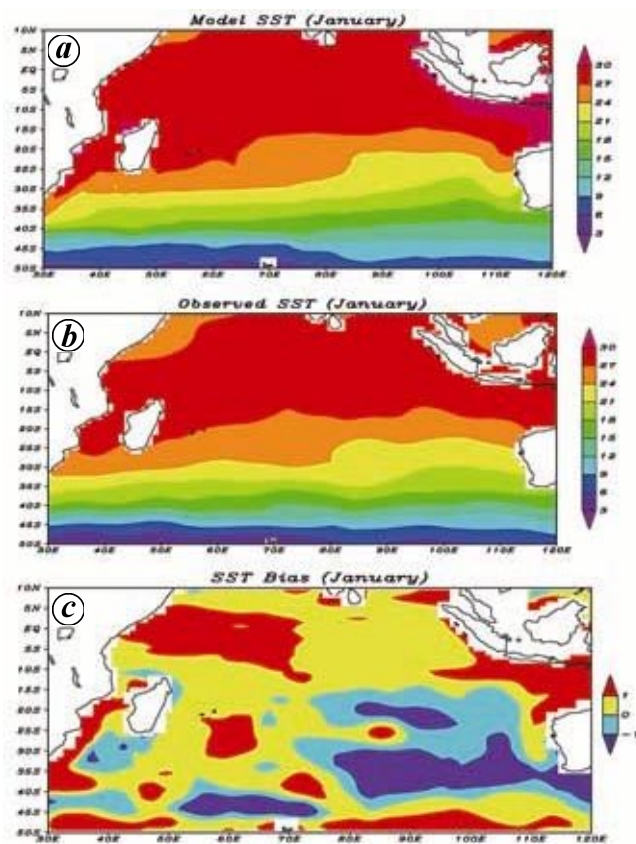


**Figure 6.** a, Time-mean (1900–25) SST ( $^\circ\text{C}$ ) simulated by the ocean model for January. b, SST (observed) for January. Contour interval is  $3.0^\circ\text{C}$ . c, SST bias between model and Levitus climatology. (Contour interval is  $1.0^\circ\text{C}$ .)

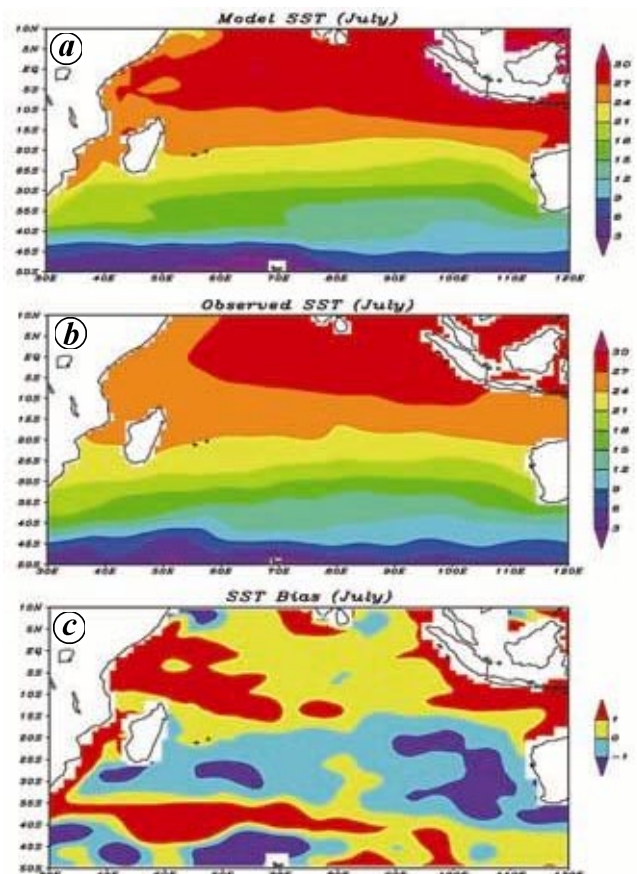


**Figure 7.** a, Time-mean (1900–25) SST ( $^\circ\text{C}$ ) simulated by the ocean model for July. b, SST (observed) for July. Contour interval is  $3.0^\circ\text{C}$ . c, SST bias between model and Levitus climatology. (Contour interval is  $1.0^\circ\text{C}$ .)

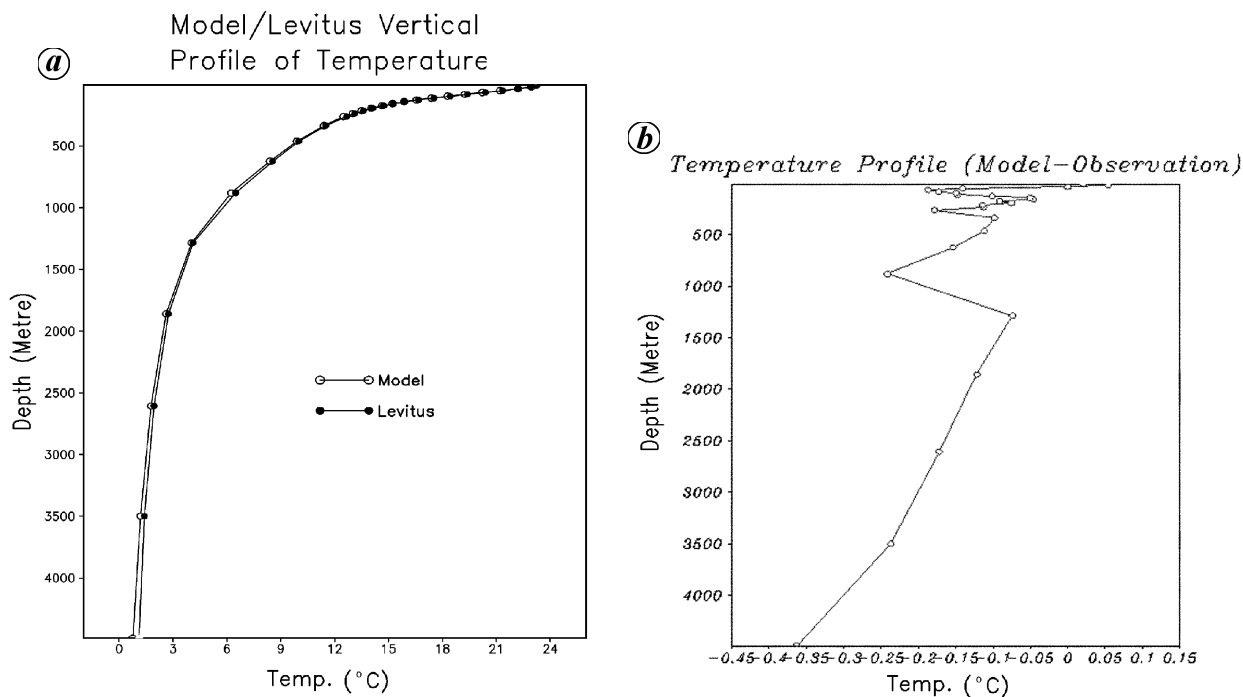


**Figure 8.** Vertical profile of temperature calculated from values averaged over the model domain (30°E–120°E, 50°S–10°N). *a*, Superimposed plot (black line is the 5 yr model climatology for years 21–25 and the green line is the Levitus climatology<sup>12</sup>). *b*, Model minus Levitus vertical profile of temperature.

Moreover, the SST distribution is approximately zonal (the isotherms are oriented roughly east-west; Figures 6 *a*, *b* and 7 *a*, *b*), with the highest values at low latitudes and lowest values at higher latitudes, corresponding closely with the input of short-wave radiation<sup>33</sup>.

In order to evaluate the model climate drift during the simulation, we examined an area-averaged vertical profile of temperature. Five-year average model climatology for years 21–25 is compared with the area-averaged vertical profile of climatological temperature in the Levitus climatology<sup>12</sup> for the same region. The model and Levitus climatology profiles given in Figure 8 *a* show that the observations are well simulated by the model. As far as the mixed-layer thermocline is concerned, the model climate drift is small relative to the climatological data<sup>12</sup>. This is also evidenced in a study in which model climate drift remained large during the first few years of the model run and decreased in subsequent years of the run<sup>34</sup>. Figure 8 *b* shows that there is oscillation in the difference of the vertical profiles of temperature between the model and the observation, which may be because of the coarser resolution of the model and numerical interpolation error.

## Conclusions

It is not possible to observe all parts of the oceans throughout the world. Therefore, we have used observations in a part of the SIO to simulate what would be happening through-

out the oceans in the present domain using a numerical OGCM and compared the simulated results with the observations. As a preliminary analysis of the OGCM, only model-simulated horizontal sea surface velocity and SST field in the SIO have been investigated and compared with the respective observed climatological datasets. Results show that the model-reproduced monthly mean circulation fields are in agreement with the observed data. The annual mean flow pattern is also in agreement with the annual mean observed field. However, a substantial decrease in the strength of the current is seen with respect to observations. The RMSE evaluated between model and observation shows that the model perform well in deep-water regions and to some extent in shallow-water regions, as evidenced by the standard deviation of the observed data. The SST field is also found to be in agreement with the observed Levitus climatology<sup>12</sup>. However, the modelled SST shows bias at some places with respect to the observations, which may be because of the coarser resolution of the model domain, as well as some deficiency in the forcing field and model configuration. In particular, SST bias is found within  $\pm 1^\circ\text{C}$  in most of the domains, except some regions in southern Arabian Sea and south of Java Sea during January and July, reflecting that the ocean model has a warm bias along the coasts and cool bias away from the coasts (near the middle of the ocean). The SST bias is again related to the model configuration and resolution, and in turn may also be related to the ocean current bias (which we cannot estimate because of

lack of ocean current observations). The area-averaged vertical profile of temperature corresponding to the model years for 21st to 25th is well simulated and shows that the model climate drift is almost negligible with respect to the Levitus climatology. Due to lack of data in the SIO, comparison with the model has to be dealt with qualitatively. However, quantitative assessments have also been performed to estimate the model performance. In brief, the study shows that model-simulated SSC and temperature fields are validated against the observations with some accuracy.

1. Chassignet, E. P. and Verron, J., In *Ocean Modelling and Parameterization (NATO Science Series) Series-C: Mathematical and Physical Sciences*, Kluwer, The Netherlands, 1998, vol. 516, p. 451.
2. Dickey, T. D., Plueddemann, A. J. and Weller, R. A., Current and water property measurements in the coastal ocean. In *The Sea* (eds Brink, K. H. and Robinson, A. R.), John Wiley, 1998, vol. 10, pp. 367–398.
3. Weller, R. A. and Davis, R. E., A vector measuring current meter. *Deep-Sea Res. A*, 1980, **27**, 565–582.
4. Pinkel, R., Acoustic Doppler techniques. In *Air–Sea Interactions, Instruments and Methods* (eds Dobson, F., Hasse, L. and Davis, R.), Plenum Press, 1980, pp. 171–199.
5. Gordon, R. L., *Acoustic Doppler Current Profiler: Principles of Operation*, A Practical Primer, RD Instruments, 1996, 2nd edn, p. 54.
6. Halpern, D., Weller, R. A., Briscoe, M. G., Davis, R. E. and McCullough, J. R., Intercomparison tests of moored current measurements in the upper ocean. *J. Geophys. Res.*, 1981, **86**, 491–528.
7. Beardsley, R. C., A comparison of the vector-averaging current meter and new Edgerton, Germeshausen, and Grier, Inc., vector measuring current meter on a surface mooring in Coastal Ocean Dynamics Experiment 1. *J. Geophys. Res.*, 1987, **92**, 1845–1859.
8. Irish, J. D., Plueddemann, A. J. and Lentz, S. Z., *In situ* comparisons of moored acoustic Doppler profilers with conventional VACM and VMCM current meters. In Proceedings of the IEEE Fifth Working Conference on Current Measurement, IEEE, St. Petersburg, FL, 1995, pp. 59–64.
9. Lumpkin, R., Matano, R. P. and Beal, K. L., 2005, Manuscript under preparation.
10. Lumpkin, R., Decomposition of surface drifter observations in the Atlantic Ocean. *Geophys. Res. Lett.*, 2003, **30**, 1753–1756.
11. Mariano, A. J. and Brown, O. B., Efficient objective analysis of dynamically heterogeneous and nonstationary fields via the parameter matrix. *Deep-Sea Res.*, 1992, **39**, 1255–1271.
12. Levitus, S., World Ocean Atlas 1994: CD-ROM dataset documentation. NODC informal report no. 13, National Oceanographic Data Center, Washington, DC, USA, 1994, p. 30.
13. Mariano, A. J., Ryan, E. H., Perkins, B. D. and Smithers, S., The Mariano Global surface velocity analysis 1.0. US Coast Guard technical report, 1995, CD-D-34-95.
14. Pacanowski, R. C., Dixon, K. and Rosati, A., The GFDL modular ocean model user guide, version 1.0. Technical report 2, Geophysical Fluid Dynamical Laboratory, National Oceanic and Atmospheric Administration, Princeton, New Jersey, USA, 1993, p. 16.
15. Huang, B. and Schneider, E. K., The response of an ocean general circulation model to surface wind stress produced by an atmospheric general circulation model. *Mon. Weather Rev.*, 1995, **123**, 3059–3085.
16. Schneider, E. K., Huang, B., Zhu, Z., DeWitt, D. G., Kinter III, J. L., Kirtman, B. and Shukla, J., Ocean data assimilation, initialization, and predictions of ENSO with a coupled GCM. *Mon. Weather Rev.*, 1999, **127**, 1187–1207.
17. Smagorinsky, J., General circulation experiments with the primitive equations: I. The basic experiment. *Mon. Weather Rev.*, 1963, **91**, 99–164.
18. Redi, M. H., Oceanic isopycnal mixing by coordinate rotation. *J. Phys. Oceanogr.*, 1982, **12**, 1154–1158.
19. Gent, P. R. and McWilliams, J. C., Isopycnal mixing in ocean circulation models. *J. Phys. Oceanogr.*, 1990, **20**, 150–155.
20. Large, W. G., McWilliams, J. C. and Doney, S. C., Oceanic vertical mixing: A review and a model with nonlocal boundary layer parameterization. *Rev. Geophys.*, 1994, **32**, 363–404.
21. Levitus, S., Climatological atlas of the world ocean. NOAA Prof. Pap., 13, US Govt. Print. Off, Washington, DC, USA, 1982, p. 173.
22. Tippet, M. K., Branston, A. G., Dewitt, David. G. and Zhang, Rong-Hua, Statistical correction of tropical Pacific sea surface temperature forecasts. *J. Climate*, 2005, **18**, 5141–5162.
23. Schneider, E. K., Kirtman, B. P., DeWitt, D. G., Rosati, A., Ji, L. and Tribbia, J. J., Retrospective ENSO forecasts: Sensitivity to atmospheric model and ocean resolution. *Mon. Weather Rev.*, 2003, **131**, 3038–3060.
24. Birol, K. A., Wallcraft, A. J. and Hurlburt, H. E., Climatological SST and MLD prediction from a global layered ocean model with an embedded mixed layer. *J. Atmos. Ocean Technol.*, 2003, **20**, 1616–1632.
25. Kalnay, E. *et al.*, The NCEP/NCAR 40-year reanalysis project. *Bull. Am. Meteorol. Soc.*, 1996, **77**, 437–470.
26. Marchuk, G. I. and Sarkisyan, A. S., In *Mathematical Modelling of Ocean Circulation*, Springer Verlag, Moscow, 1988, p. 292.
27. Gandin, L. S., In *Objective Analysis of Meteorological Fields*. Translated from Russian by the Israel program for scientific translations (1965), 1963, p. 242.
28. Thiebaux, J. J. and Pedder, M. A., Producing accurate maps of Gulf stream thermal fronts using objective analysis. *J. Geophys. Res. C*, 1989, **94**, 8040–8052.
29. Bretherton, F. P., Davis, R. E. and Fandry, C. B., A technique for objective analysis and design of oceanographic experiments applied to MODE-73. *Deep-Sea Res.*, 1976, **23**, 559–582.
30. Carter, E. F. and Robinson, A. R., Analysis models for the estimation of oceanic fields. *J. Atmos. Ocean Technol.*, 1987, **4**, 49–74.
31. Richardson, P. L., Drifting in the wind: Leeway error in shipdrift data. *Deep-Sea Res.*, 1997, **44**, 1877–1903.
32. Behra, S. K., Salvekar, P. S. and Yamagata, T., Simulation of inter-annual SST variability in the tropical Indian Ocean. *J. Climate*, 2000, **113**, 3487–3499.
33. George, P. L. and Emery, W. J., In *Descriptive Physical Oceanography*, Pergamon Press, Oxford, 1982, 14th edn, p. 249.
34. Ezer, T. and Mellor, G. L., Simulation of the Atlantic Ocean with a free surface sigma coordinate ocean model. *J. Geophys. Res.*, 1997, **102**, 15647–15657.

ACKNOWLEDGEMENTS. We thank Drs Ben Kirtman and Bohua Huang, Center of Ocean Land Atmosphere Studies (COLA), Maryland, USA for providing the Modular Ocean Model (MOM3.0) source code, and for their suggestions. We also thank Dr P. C. Pandey, Ex-Director, NCAOR, Goa, for encouragement and thank to NCAOR, Goa for providing financial assistance in the form of a research project. We are grateful to Dr Arthur J. Mariano, University of Miami, USA and Dr Rick Lumpkin, NOAA, USA for providing the observed velocity field for the region 50°S–10°N, 30–120°E. We thank the anonymous reviewers for their suggestions.

Received 2 December 2005; revised accepted 22 January 2007